

# Fast and Radiation Hard Inorganic Scintillators for Future HEP Experiments

Chen Hu, Liyuan Zhang, and Ren-Yuan Zhu

HEP Crystal Laboratory, California Institute of Technology, Pasadena, CA 91125, USA

## 1. Introduction

Future HEP experiments at the energy and intensity frontiers require fast and ultrafast inorganic scintillators with excellent radiation hardness to face the challenges of unprecedented event rate and severe radiation environment. We report recent progress in fast and ultrafast inorganic scintillators for future HEP experiments. Examples are LYSO crystals and LuAG ceramics for an ultra-compact shashlik sampling calorimeter for the HL-LHC and the proposed FCC-hh, and yttrium doped BaF<sub>2</sub> crystals for the proposed Mu2e-II experiment. Applications for Gigahertz hard X-ray imaging will also be discussed.

Table I shows scintillation performance of fast and ultrafast inorganic scintillators. LYSO crystals and LuAG:Ce ceramics show high stopping power, high light output, short decay time and good radiation hardness against ionization dose and hadrons. Yttrium doped BaF<sub>2</sub> crystal shows ultrafast scintillation light with sub-ns decay time and a suppressed slow scintillation light. These inorganic scintillators are promising for future HEP experiments.

Table I Scintillation Performance of Fast and Ultrafast Inorganic Scintillators

	BaF <sub>2</sub>	BaF <sub>2</sub> :Y	ZnO:Ga	YAP:Yb	YAG:Yb	$\beta$ -Ga <sub>2</sub> O <sub>3</sub>	LYSO:Ce	LuAG:Ce	YAP:Ce	GAGG:Ce	LuYAP:Ce	YSO:Ce
Density (g/cm <sup>3</sup> )	4.89	4.89	5.67	5.35	4.56	5.94 <sup>a</sup>	7.4	6.76	5.35	6.5	7.2 <sup>f</sup>	4.44
Melting points (°C)	1280	1280	1975	1870	1940	1725	2050	2060	1870	1850	1930	2070
X <sub>0</sub> (cm)	2.03	2.03	2.51	2.77	3.53	2.51	1.14	1.45	2.77	1.63	1.37	3.10
R <sub>M</sub> (cm)	3.1	3.1	2.28	2.4	2.76	2.20	2.07	2.15	2.4	2.20	2.01	2.93
$\lambda_1$ (cm)	30.7	30.7	22.2	22.4	25.2	20.9	20.9	20.6	22.4	21.5	19.5	27.8
Z <sub>eff</sub>	51.6	51.6	27.7	31.9	30	28.1	64.8	60.3	31.9	51.8	58.6	33.3
dE/dX (MeV/cm)	6.52	6.52	8.42	8.05	7.01	8.82	9.55	9.22	8.05	8.96	9.82	6.57
$\lambda_{peak}^a$ (nm)	300 220	300 220	380	350	350	380	420	520	370	540	385	420
Refractive Index <sup>b</sup>	1.50	1.50	2.1	1.96	1.87	1.97	1.82	1.84	1.96	1.92	1.94	1.78
Normalized Light Yield <sup>c,d</sup>	42 4.8	1.7 4.8	6.6 <sup>d</sup>	0.19 <sup>d</sup>	0.36 <sup>d</sup>	6.5 (7.0±0.2)×10 <sup>d</sup>	100 (5.6±0.2)×10 <sup>d</sup>	35 <sup>d</sup> 48 <sup>d</sup>	32 36.6±0.7	115 35.6±0.8	16 15	80
Total Light yield (ph/MeV)	13,000	2,000	2,000 <sup>d</sup>	57 <sup>d</sup>	110 <sup>d</sup>	2,100	30,000	25,000 <sup>d</sup>	12,000	34,400	10,000	24,000
Decay time <sup>e</sup> (ns)	600 0.5	600 0.5	<1	1.5	4	148 6	40	820 50	191 25	53	1485 36	75
LY in 1st ns (photons/MeV)	1200	1200	610 <sup>d</sup>	28 <sup>d</sup>	24 <sup>d</sup>	43	740	240	391	640	125	318
40 keV Att. Leng. (1/e, mm)	0.106	0.106	0.407	0.314	0.439	0.394	0.185	0.251	0.314	0.319	0.214	0.334

## 2. Bright, Fast and Radiation Hard LYSO:Ce and LuAG:Ce

### 2.1 LYSO:Ce Crystals and LuAG:Ce Ceramics

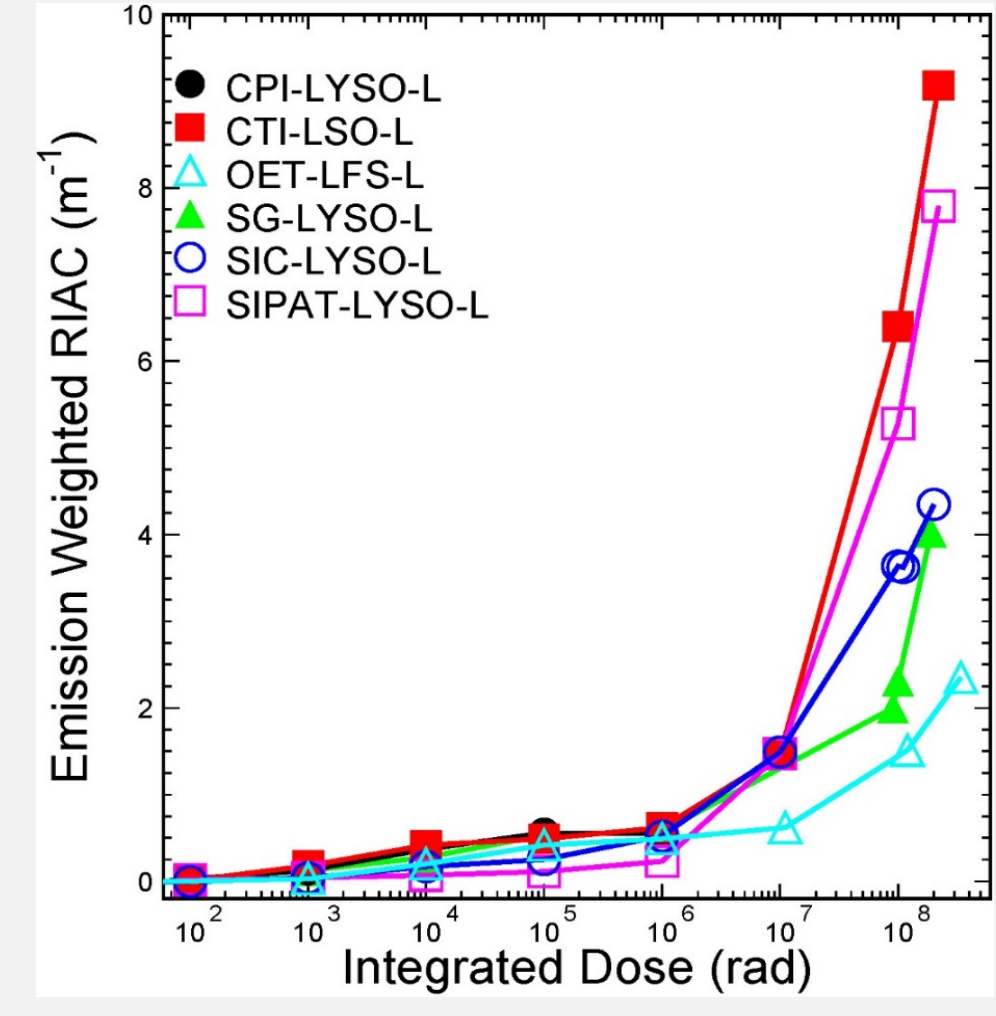


Fig. 1 Emission weighted RIAC values as a function of integrated dose for 20 cm long LYSO crystals from various vendors.

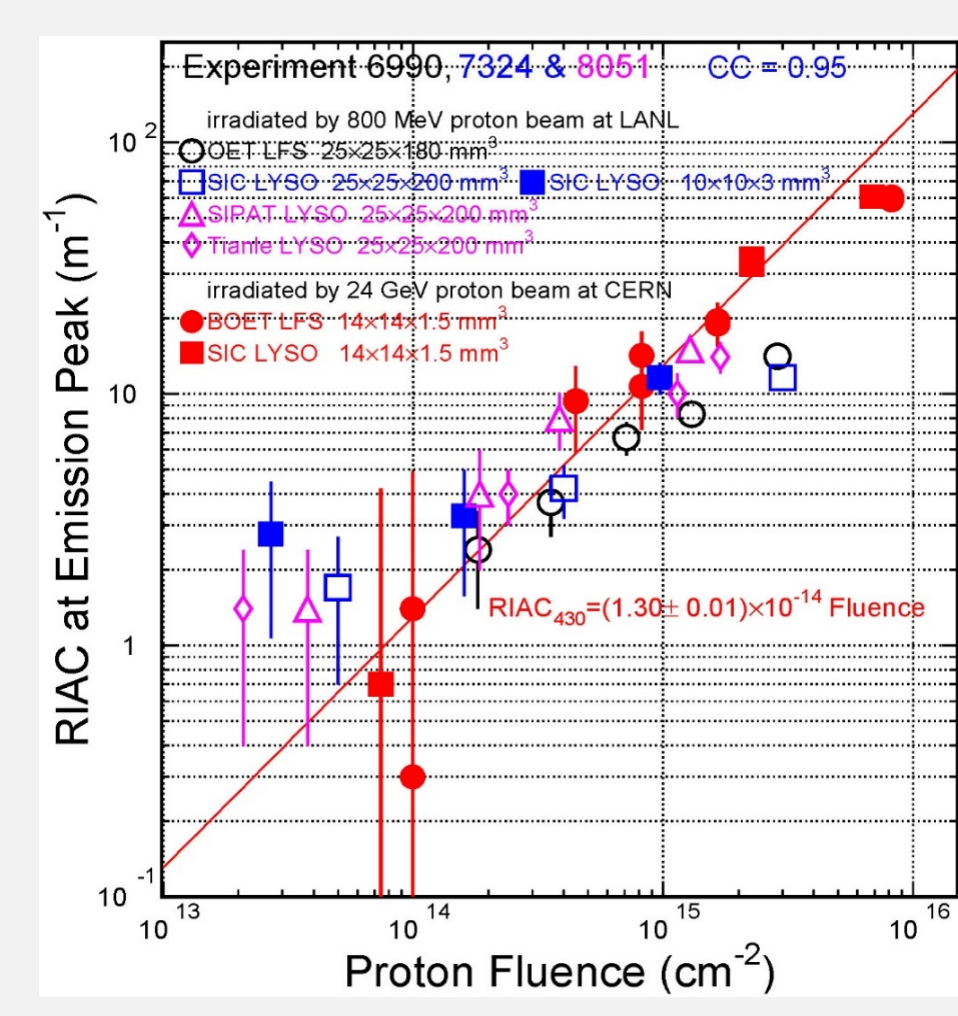


Fig. 2 The RIAC values as a function of proton fluence for LYSO crystals from various vendors.

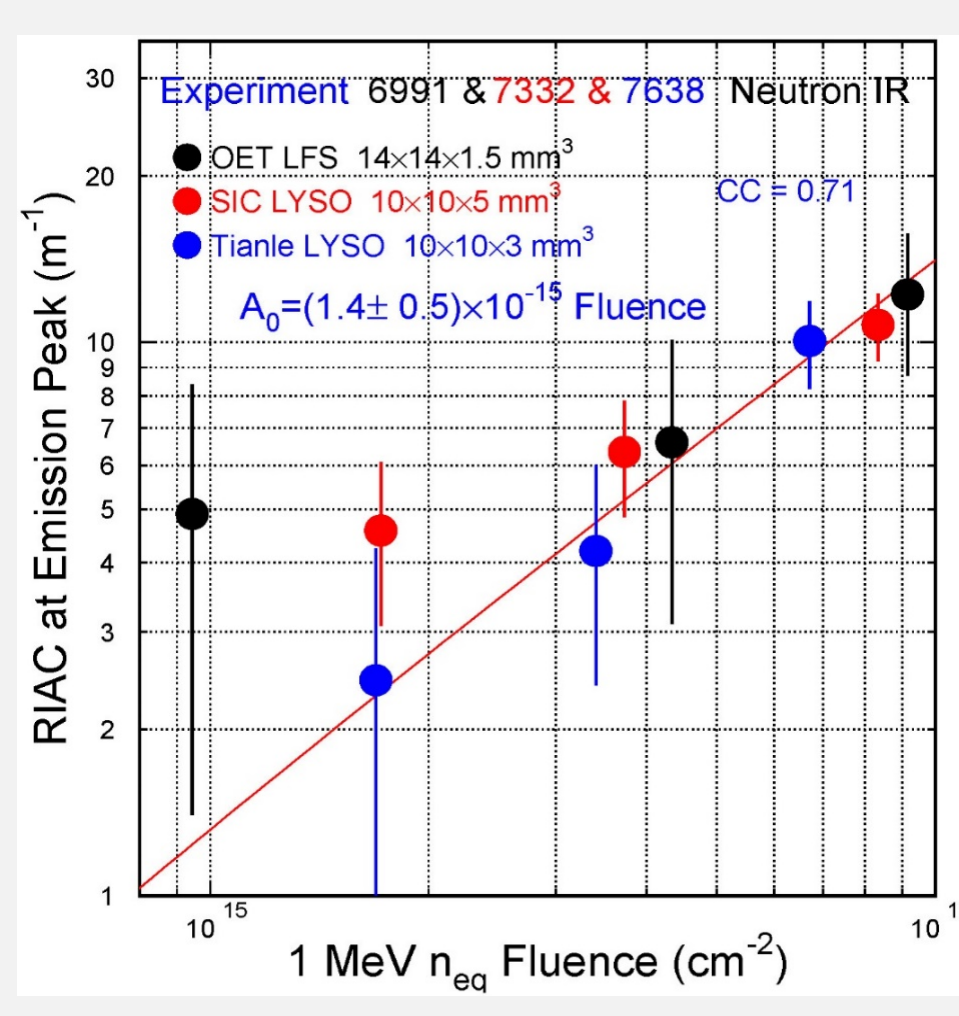


Fig. 3 The RIAC values as a function of 1 MeV equivalent neutron fluence for LYSO crystals from various vendors.

Figs. 1, 2, and 3 show respectively the radiation induced absorption coefficient (RIAC) values as a function of (1) integrated dose, (2) proton fluence, and (3) 1 MeV equivalent neutron fluence for LYSO crystals from various vendors. We found that damage induced by protons is an order of magnitude larger than that from neutrons due to ionization energy loss in addition to displacement and nuclear breakup. These results prove that LYSO crystals from different vendors satisfy CMS BTL specification: RIAC < 3 / m after 4.8 Mrad, 2.5 × 10<sup>3</sup> p/cm<sup>2</sup> and 3 × 10<sup>14</sup> n<sub>eq</sub>/cm<sup>2</sup>.

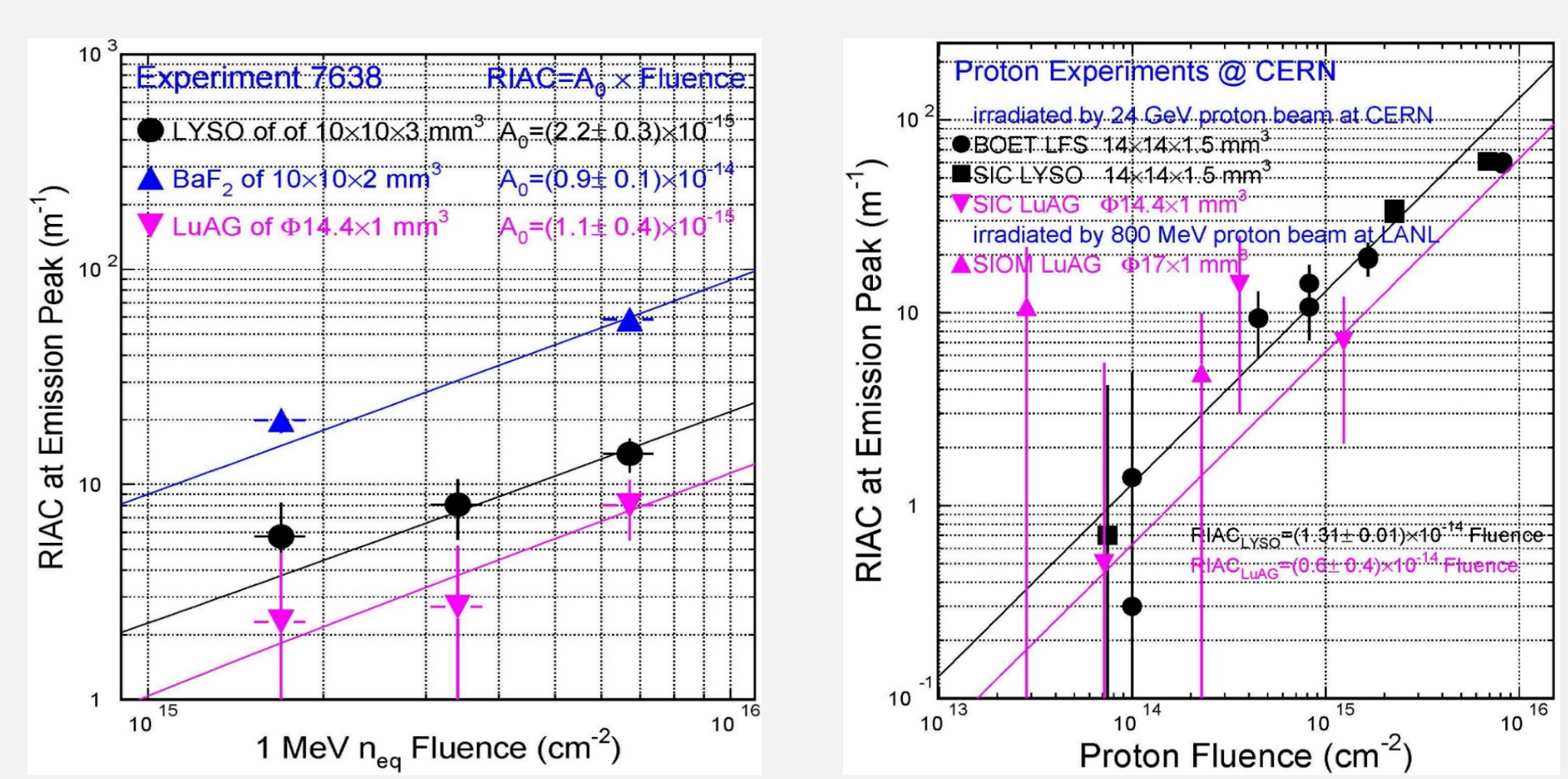


Fig. 4 The RIAC values as a function of (1) 1 MeV equivalent neutron fluence and (2) proton fluence for LuAG:Ce ceramics and LYSO crystals. We found that LuAG:Ce ceramics show a factor of two better radiation hardness than LYSO crystals up to 6.7 × 10<sup>15</sup> n<sub>eq</sub>/cm<sup>2</sup> and 1.2 × 10<sup>15</sup> p/cm<sup>2</sup>, so are promising for the FCC-hh. Fig. 6 shows that Ca<sup>2+</sup> co-doping improves the Fast/Total (F/T) ratio to 90%.

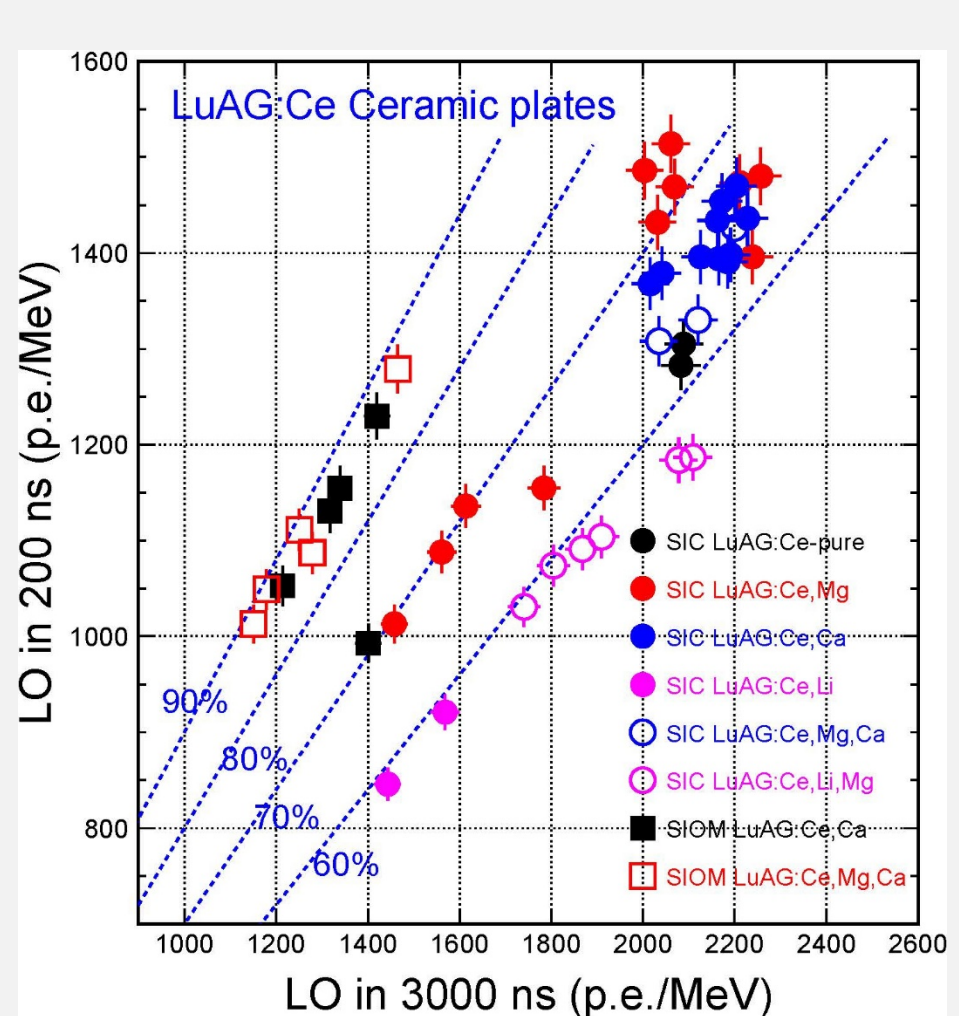


Fig. 5 The RIAC values as a function of proton fluence for LYSO crystals and LuAG:Ce ceramics.

Figs. 4 and 5 show the RIAC values as a function of (1) 1 MeV equivalent neutron fluence and (2) proton fluence for LuAG:Ce ceramics and LYSO crystals. We found that LuAG:Ce ceramics show a factor of two better radiation hardness than LYSO crystals up to 6.7 × 10<sup>15</sup> n<sub>eq</sub>/cm<sup>2</sup> and 1.2 × 10<sup>15</sup> p/cm<sup>2</sup>, so are promising for the FCC-hh. Fig. 6 shows that Ca<sup>2+</sup> co-doping improves the Fast/Total (F/T) ratio to 90%.

## 2.2 $\gamma$ -Ray and Neutron Induced Readout Noise in LYSO+SiPM Packages

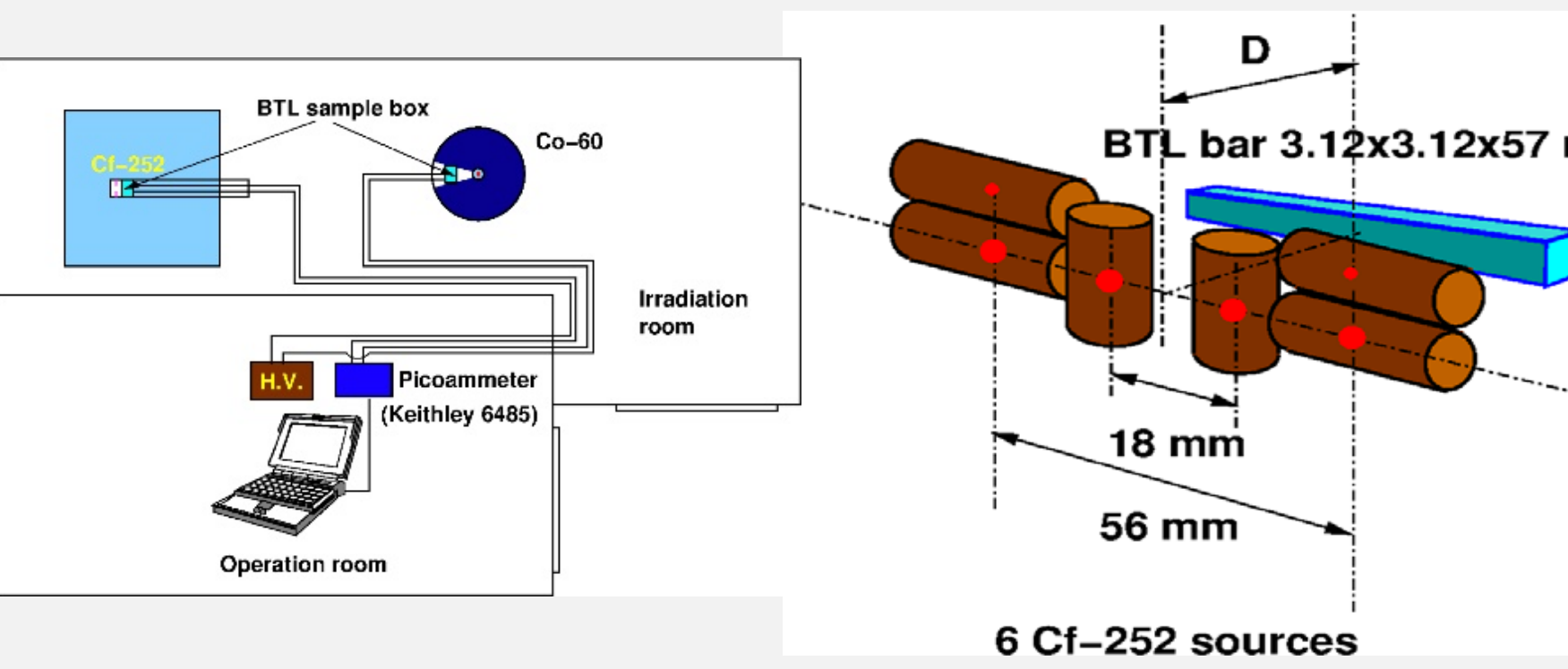


Fig. 7 The setup used to measure radiation induced photocurrent and readout noise (RIN) in LYSO+SiPM before, during and after irradiation.

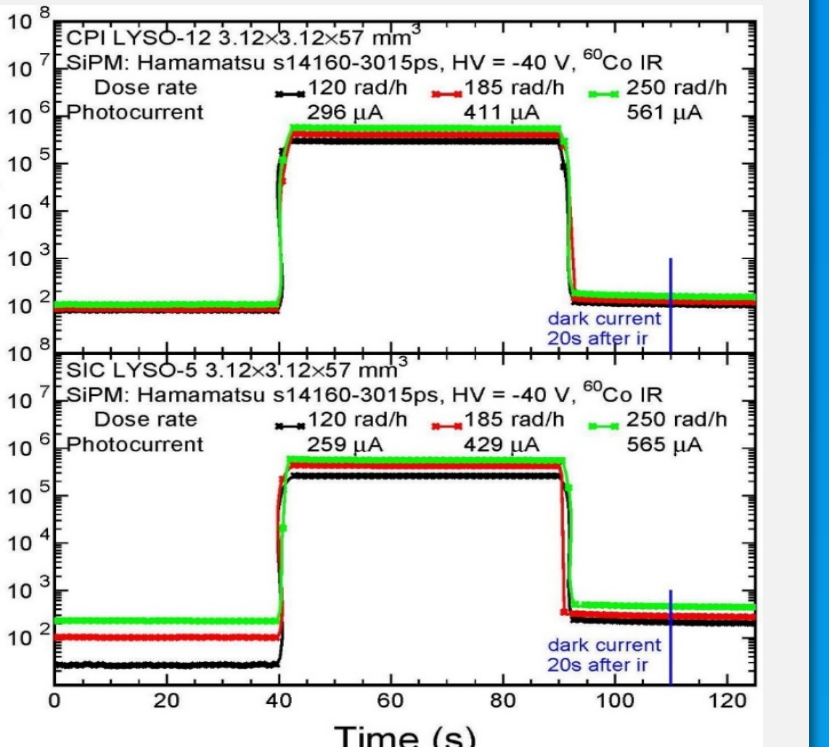


Fig. 8 Three Cf-252 source pairs used as the neutron source to measure the neutron induced photocurrent and readout noise in LYSO+SiPM packages.

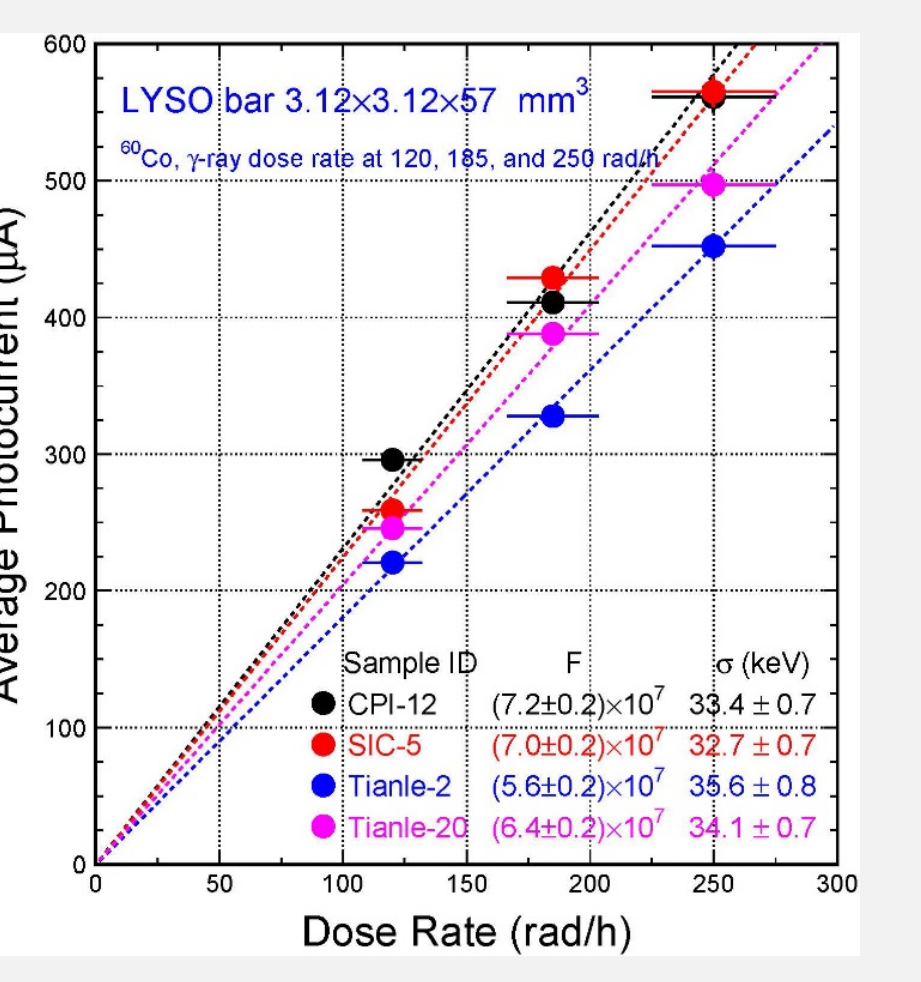


Fig. 9 Histories of the SiPM photocurrent for CPI-12 (top) and SIC-5 (bottom) LYSO bars under Co-60 y-ray irradiation.

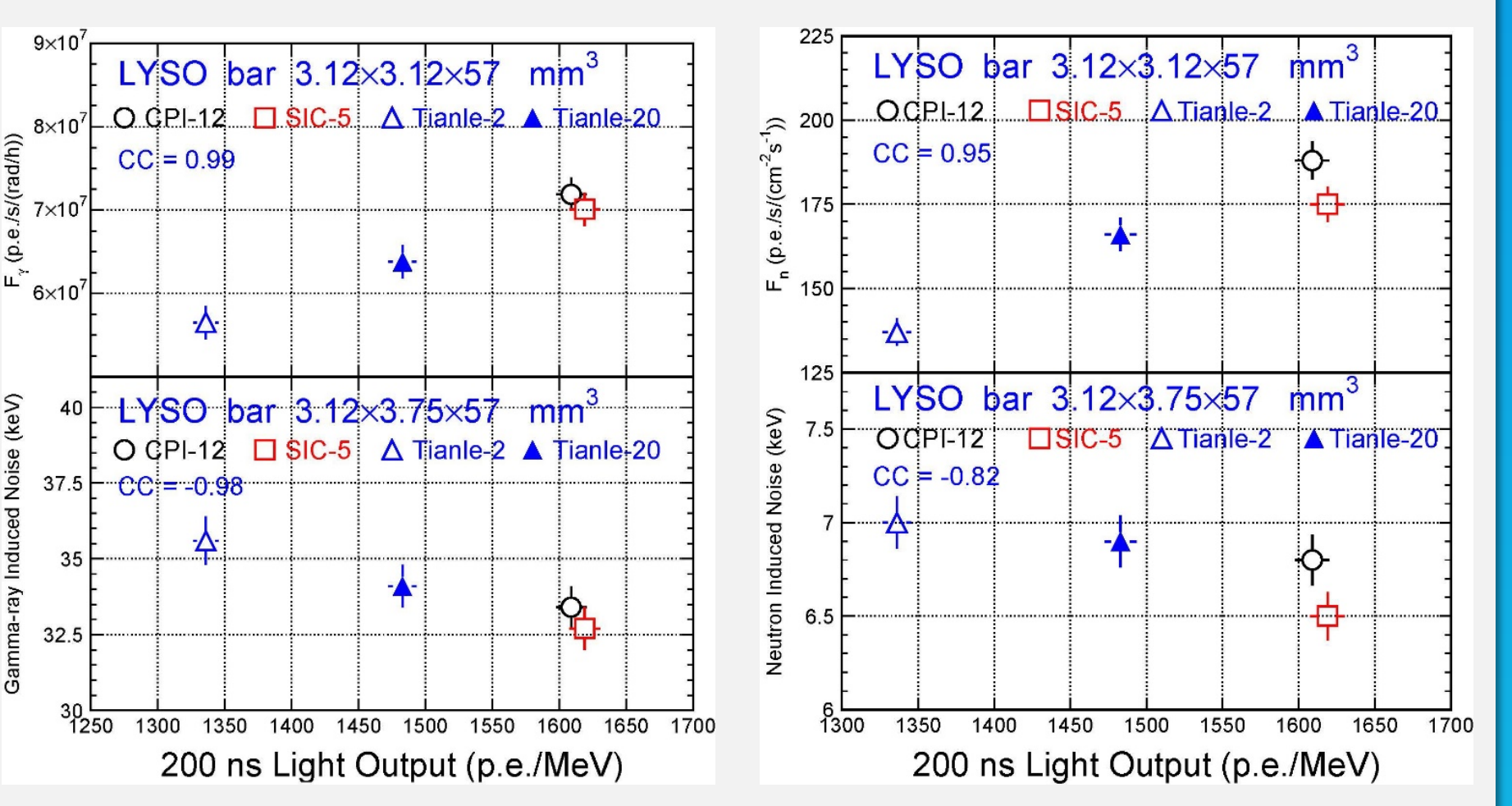


Fig. 10 Photocurrent is shown as a function of the dose rate for four LYSO+SiPM packages.

Fig. 11 Correlation between F<sub>y</sub> (top) and RIN:y (bottom) vs. the LO in 200 ns for four LYSO+SiPM packages.

Fig. 11 Correlation between F<sub>n</sub> (top) and RIN:n (bottom) vs. the LO in 200 ns for four LYSO+SiPM packages.

Fig. 12 Correlation between F<sub>n</sub> (top) and RIN:n (bottom) vs. the LO in 200 ns for four LYSO+SiPM packages.

Fig. 12 Correlation between F<sub>n</sub> (top) and RIN:n (bottom) vs. the LO in 200 ns for four LYSO+SiPM packages.

Fig. 7 shows the setup for the RIN:y and RIN:n experiments. Fig. 8 shows the layout of the neutron source assembly consisting of three cylindrical Cf-252 source pairs. Fig. 9 shows histories of the photocurrent measured for CPI-12 (top) and SIC-5 (bottom) LYSO+SiPM packages under Co-60 irradiation of 120, 185 and 250 rad/h. Fig. 10 shows the photocurrent measured during irradiation as a function of the dose rate with a good linearity. Figs. 11 and 12 show an excellent correlation between the F<sub>y</sub> and F<sub>n</sub> (top) and RIN:y and RIN:n (bottom) vs. the LO in 200 ns gate, and the RIN:y and RIN:n values of about 34 and 7 keV respectively, much less than the 4.2 MeV signal expected from minimum ionization particles.

## 3.2 Slow Suppression by Yttrium Doping in BaF<sub>2</sub>

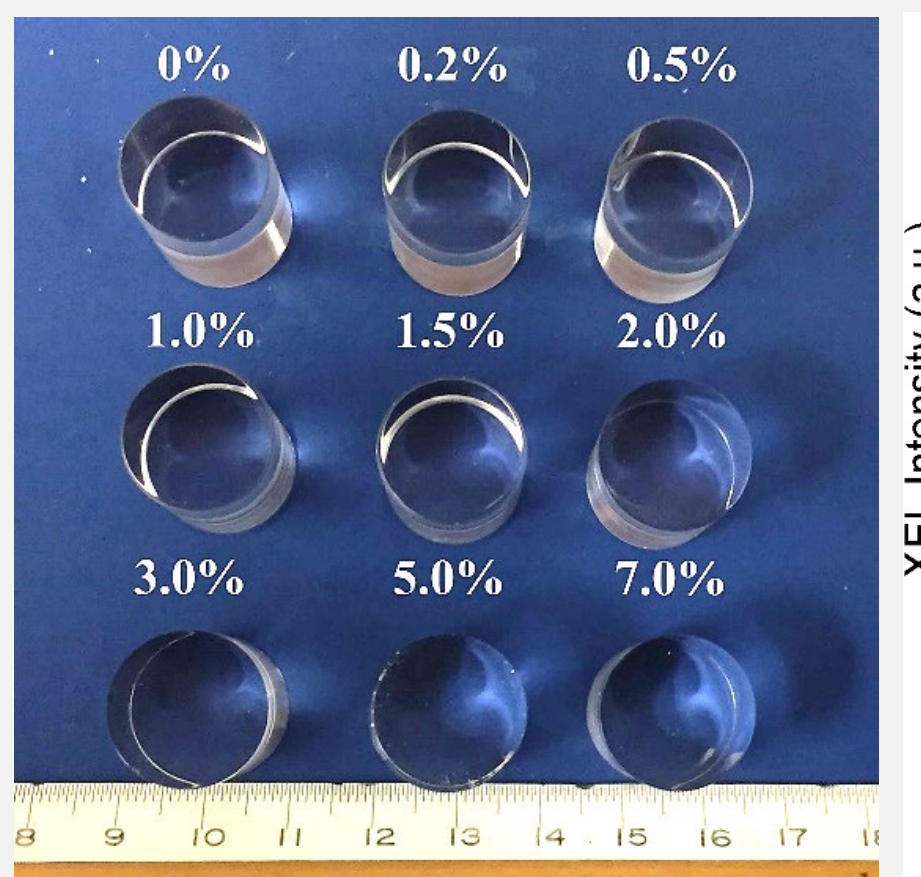


Fig. 19 Nine BaF<sub>2</sub> crystal cylinders of Φ18×21 mm<sup>3</sup> grown at BGRI with various Yttrium-doping levels.

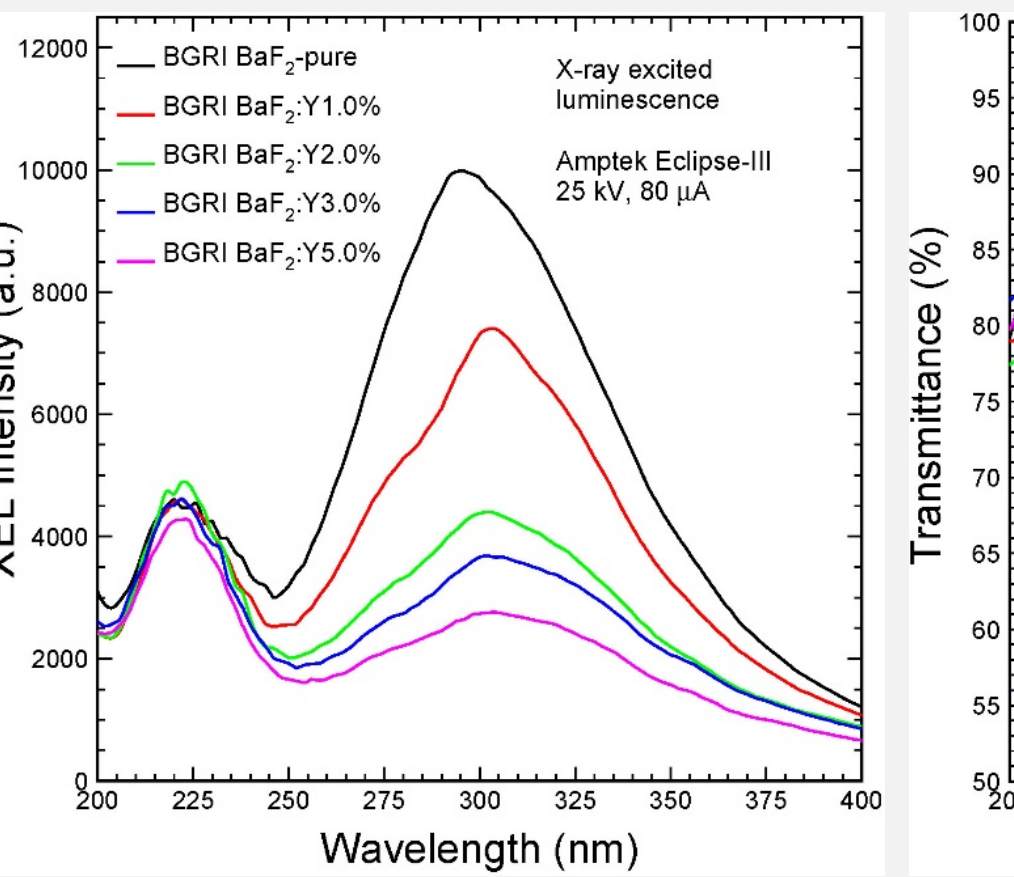


Fig. 20 XEL spectra for five BaF<sub>2</sub> cylinders with various yttrium-doping levels.

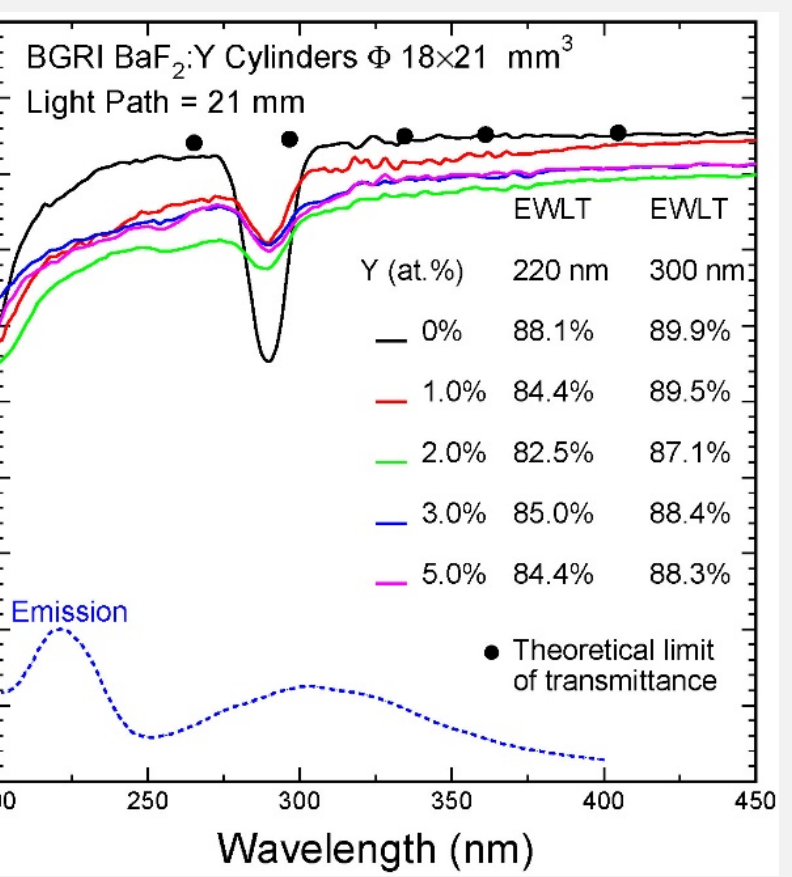


Fig. 21 Transmittance and XEL spectra for five BaF<sub>2</sub> cylinders with various yttrium-doping levels.

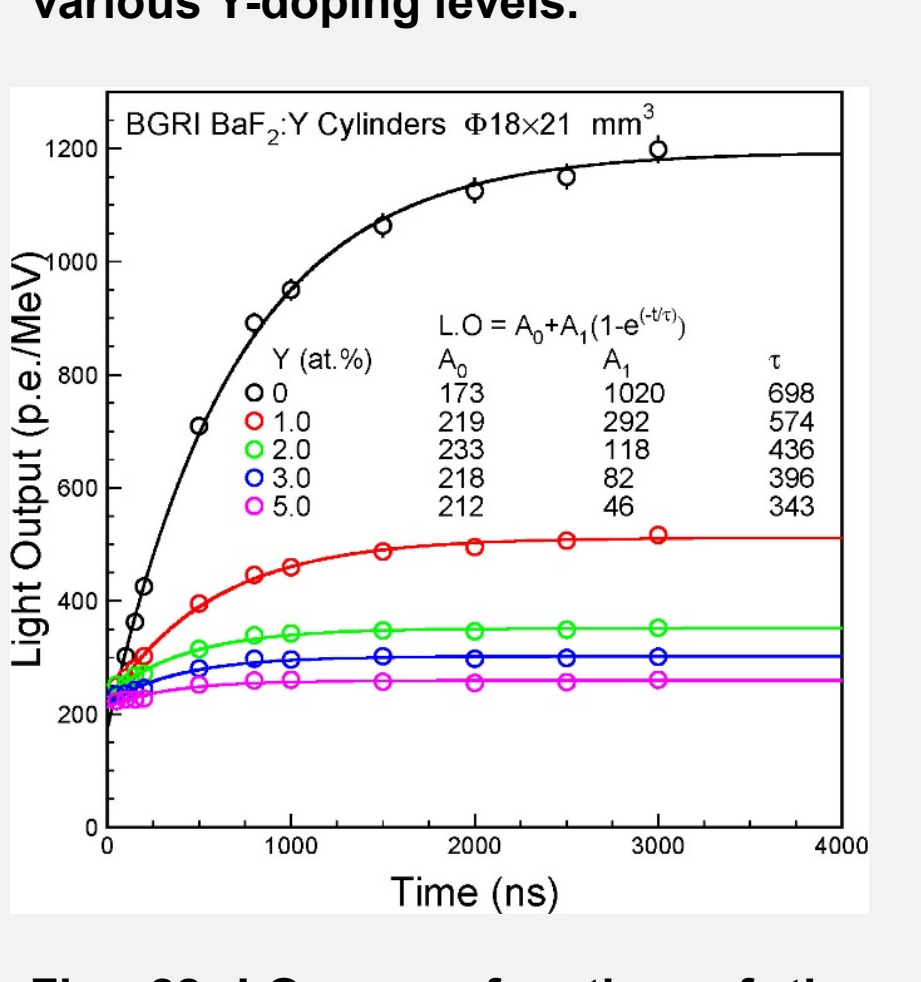


Fig. 22 LO as a function of the integration time for BaF<sub>2</sub> cylinders with different yttrium-doping levels.

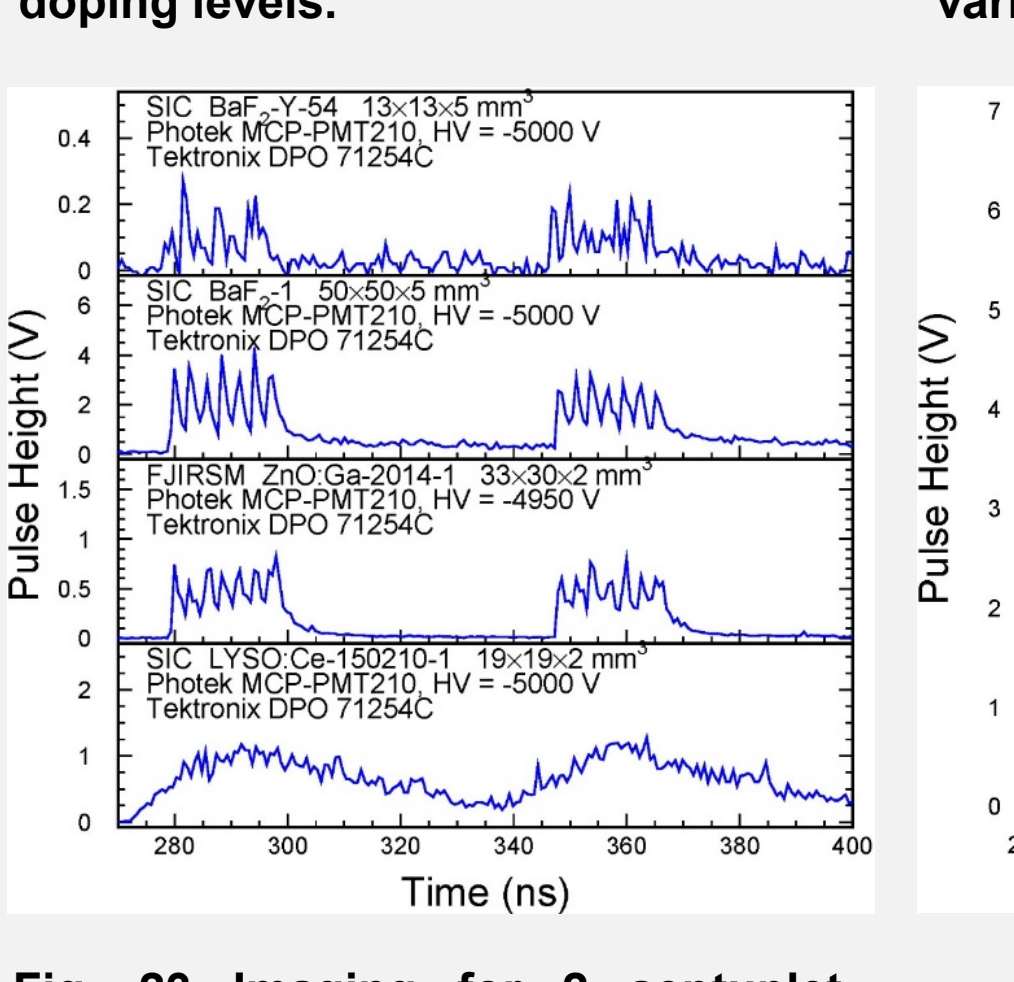


Fig. 23 Imaging for 2 septuplet bunches measured by BaF<sub>2</sub>, ZnO:Ga, and LYSO:Ce, respectively.

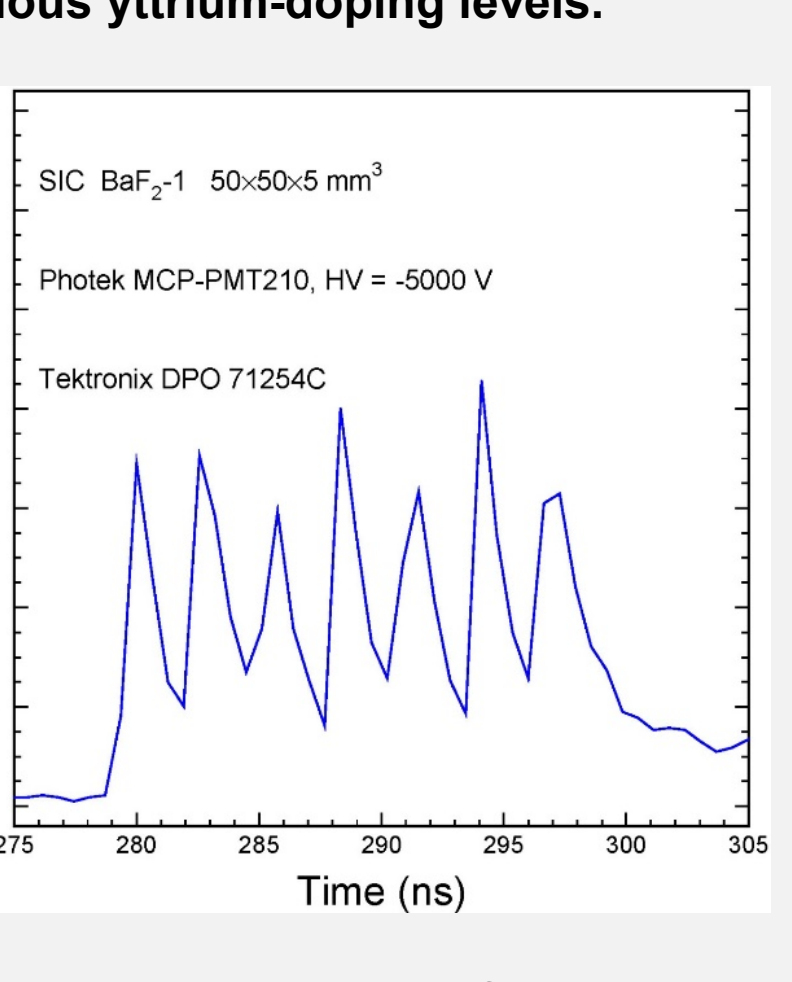


Fig. 24 BaF<sub>2</sub> imaging for 2.83 ns bunch spacing.

Fig. 19 shows nine BaF<sub>2</sub> cylinders of Φ18×21 mm<sup>3</sup> grown at BGRI with different Y<sup>3+</sup> doping levels. Fig. 20 shows the XEL peaks at 220 and 300 nm for the fast and slow light, showing a reduced slow light intensity for increased yttrium doping level, while the intensity of the fast emission is consistent. Fig. 21 shows the transmittance spectra (solid lines) measured along 21 mm light path for all samples. Fig. 22 shows LO as a function of integration time for these samples, confirming a reduced slow component and consistent fast component. Figs. 23 and 24 shows the response of BaF<sub>2</sub> and BaF<sub>2</sub>-Y to septuplet x-ray bunch with 2.83 ns bunch spacing, providing a proof of principle for the ultrafast inorganic scintillator-based front imager for GHz hard X-ray imaging.

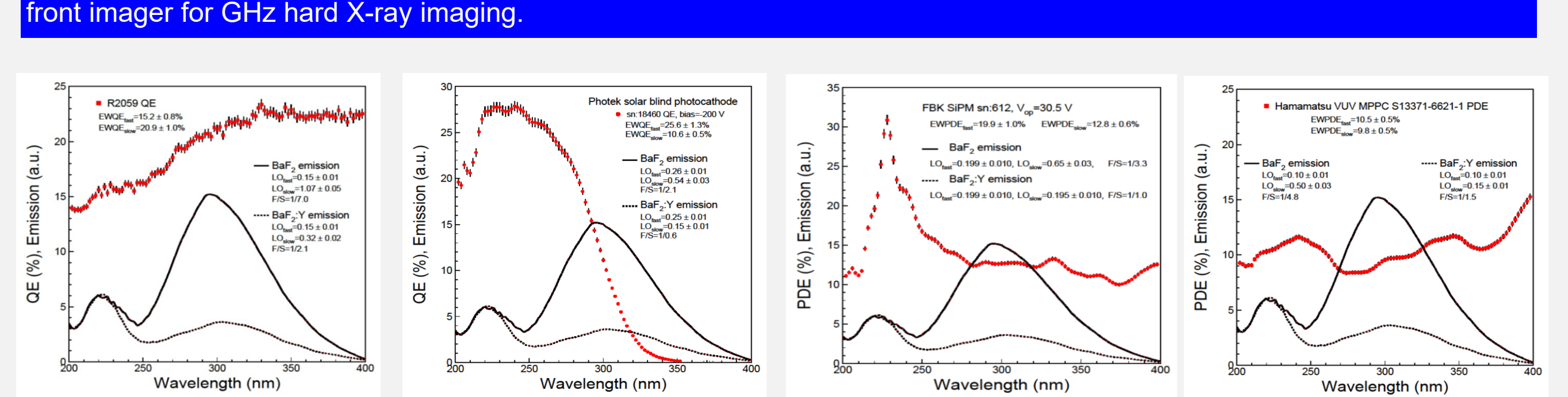


Fig. 25 shows the measured QE of four VUV photodetectors. While yttrium doping in BaF<sub>2</sub> crystals increases its F/S ratio significantly a solar-blind photodiode is also needed to minimize the pileup for a BaF<sub>2</sub> crystal based ultrafast calorimeter for future experiments, such as Mu2e-II.

## 4. Summary

- Bright, fast and radiation hard inorganic scintillators are needed for future HEP experiments at the HL-LHC and FCC-hh. Our data show that mm thick plates of LYSO:Ce crystal and LuAG:Ce ceramics survive 10<sup>15</sup> p/cm<sup>2</sup> and 10<sup>16</sup> n<sub>eq</sub>/cm<sup>2</sup>, so are promising materials in severe radiation environment.
- The RIN:y and RIN:n experiments carried out for four LYSO+SiPM packages show the RIN:y and RIN:n values of about 34 keV under 200 rad/h and 7 keV under the neutron flux of 3.2 × 10<sup>6</sup> n<sub>eq</sub>/cm<sup>2</sup>/s, which are negligible as compared to the 4.2 MeV MIP signal for the CMS BTL detector. The result also indicates that the radiation induced readout noise *in situ* is dominated by ionization dose.
- Undoped BaF<sub>2</sub> crystals provide ultrafast light with sub-ns decay time and a good radiation hardness up to 130 Mrad. Yttrium doping suppresses its slow light and promises an ultrafast inorganic scintillator with much reduced slow contamination. R&D is going for developing both yttrium doped BaF<sub>2</sub> and solar-blind VUV photodetectors for future HEP experiments, such as Mu2e-II.

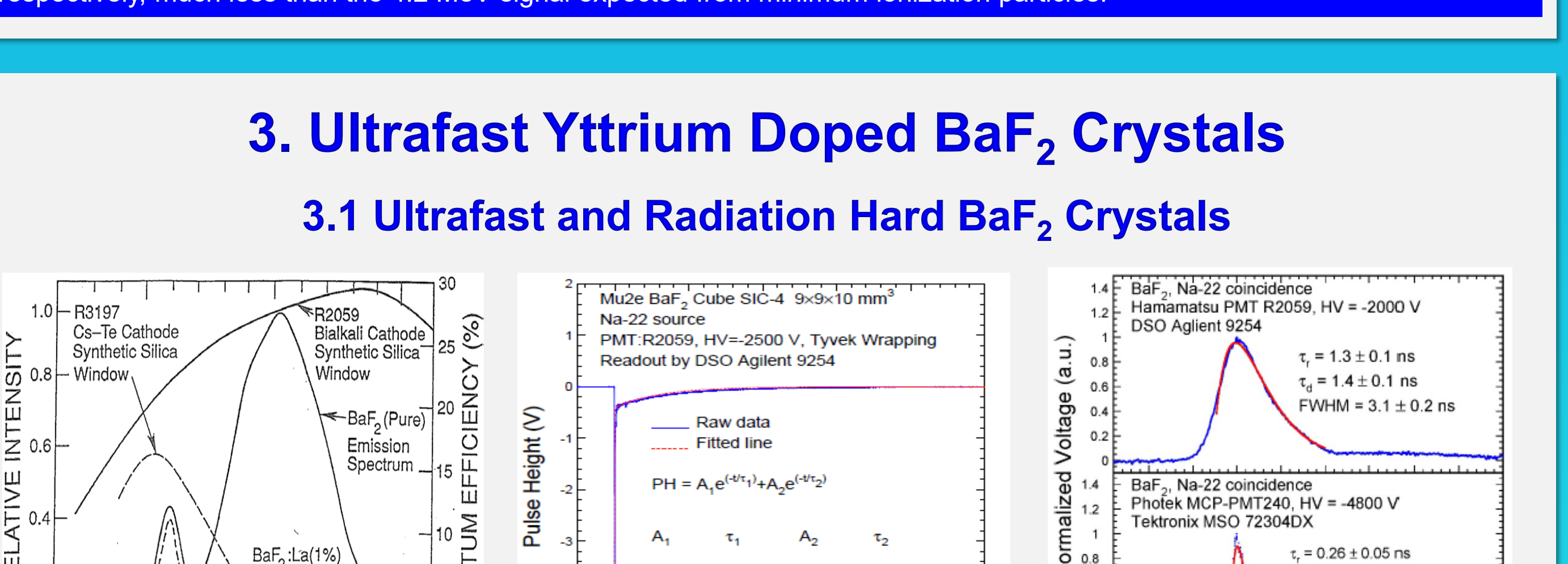


Fig. 13 BaF<sub>2</sub> emission and QE of various vacuum PMTs.

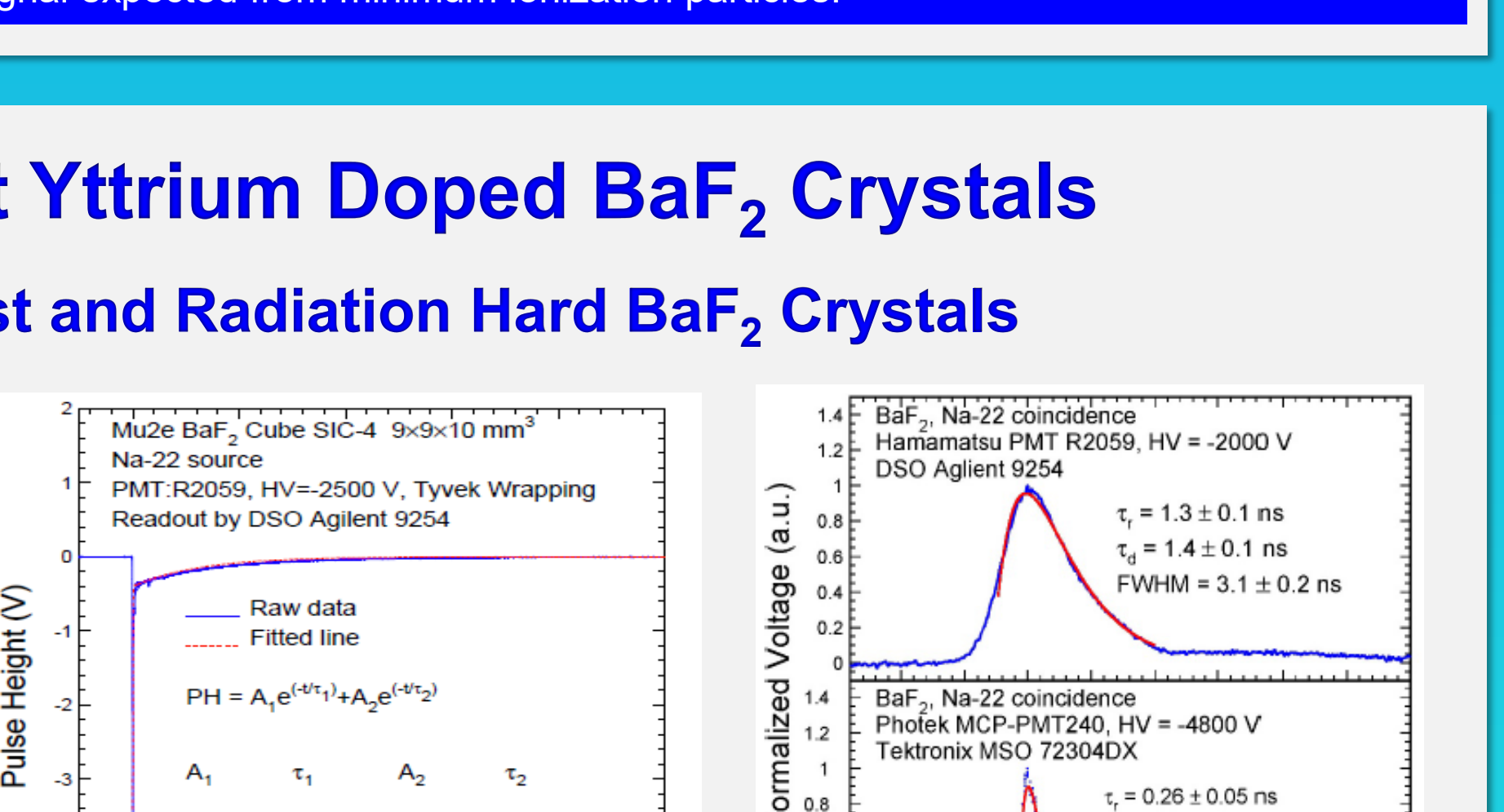


Fig. 14 Pulse shape of BaF<sub>2</sub> crystal measured by a PMT.

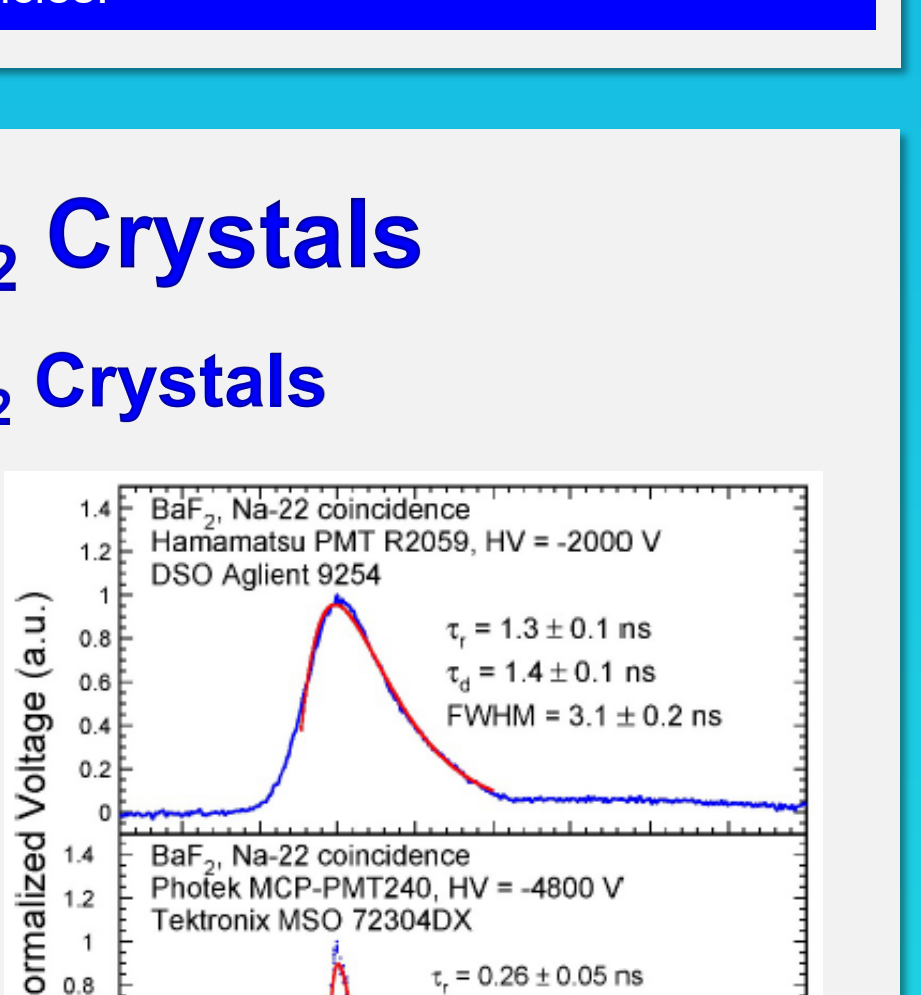


Fig. 15 Pulse shape of BaF<sub>2</sub> crystal measured by a PMT and an MCP-PMT.

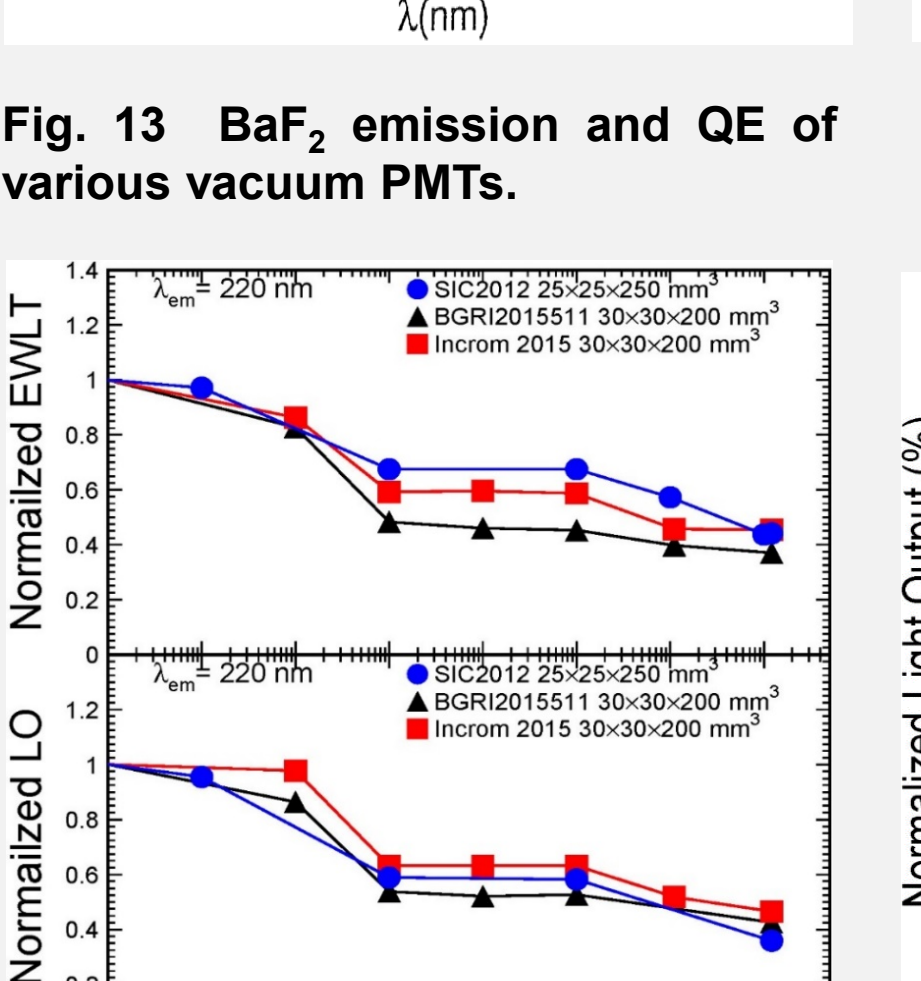


Fig. 16 Normalized EWLT and LO of 20 cm BaF<sub>2</sub> crystals up to 130 Mrad.

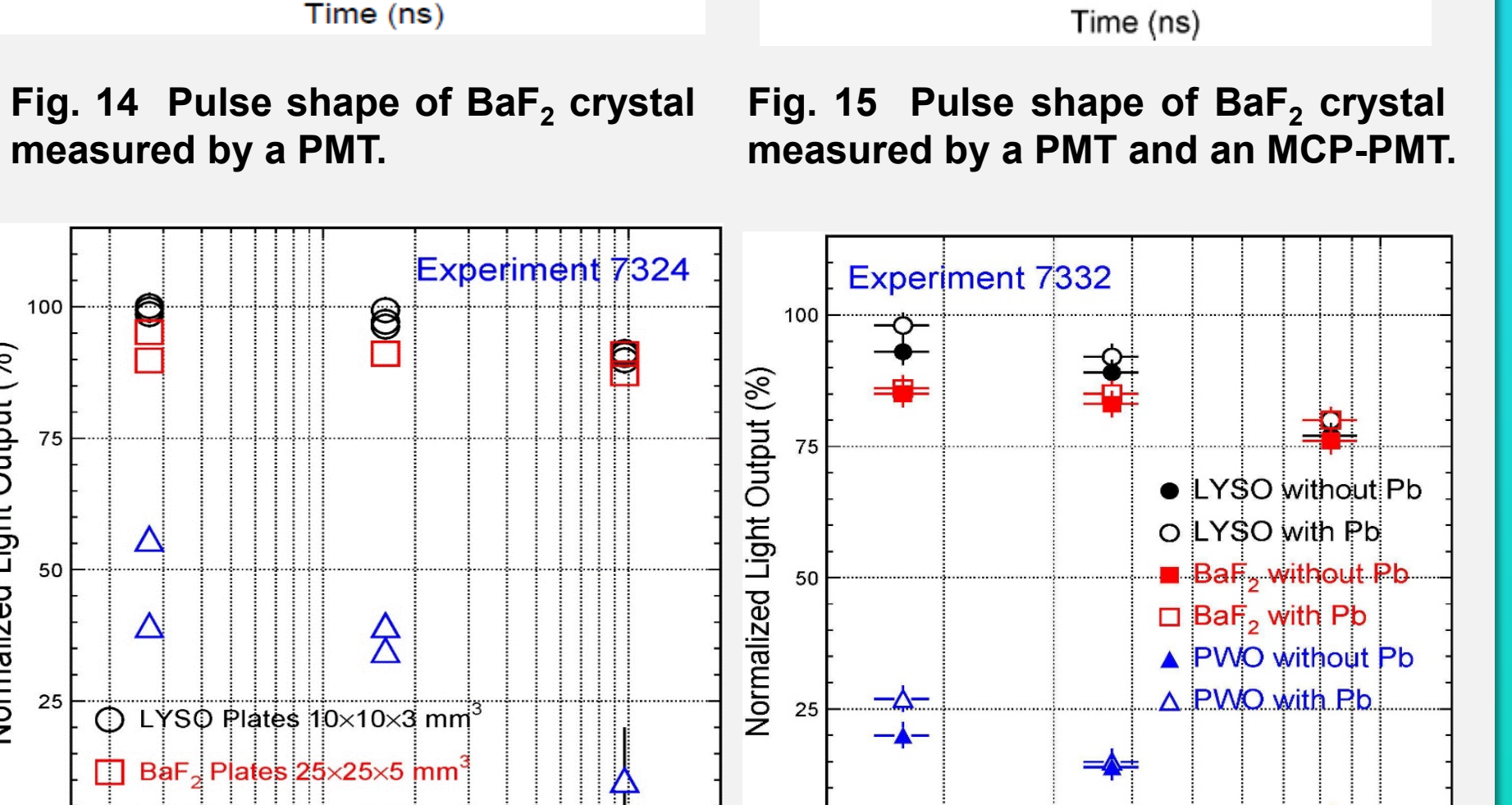


Fig. 17 Normalized LO of BaF<sub>2</sub> crystals after protons up to